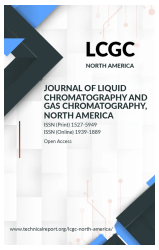

Journal of Liquid Chromatography and Gas Chromatography, North America
https://technicalreport.org/lcgcnam

LC GC N. Am., Vol. 44, No.1, 01-07, 2026

Technical Reports Press

RESEARCH ARTICLE

State-Space Analysis of Hidden Low-Conductance States and Cooperative Electrochemical Gating in the Trimeric β-Barrel Channel OmpF

Louis E. Brus[1*]

[1]*Department of Chemistry, Columbia University, New York, New York 10027, USA*
[*]*Corresponding author*

Corresponding author:
leb26@columbia.edu

Abstract

Voltage-induced closure of bacterial β-barrel channels is observed as stepwise attenuation of single-channel current, yet the physical origin of the residual low-conductance levels remains uncertain. Concentration-dependent recordings of the trimeric porin OmpF show three linked features: non-monotonic first-monomer closure across electrolyte concentration, measurable current after all three monomers occupy low-conductance configurations, and selectivity reversal from cation preference in high-conductance states to anion preference in the fully low-conductance state. These observations require analysis of complete current trajectories rather than averages of first-closure dwell time alone. This study develops a continuous-time state-space model for single-channel OmpF records with observable conductance levels L_0, L_1, L_2, and L_3, while allowing L_3 to contain multiple latent substates. The independent-monomer reference model imposes the rate constraint $q_{01} : q_{12} : q_{23} = 3 : 2 : 1$; deviations from this ratio provide a direct estimate of inter-monomer coupling. Robust current-emission and joint conductance–selectivity components distinguish instrumental noise from reproducible low-state heterogeneity. Transition intensities are linked to electrolyte concentration, voltage polarity, and cation identity, separating the concentration dependence of first closure from the conditional kinetics of later closures. The resulting analysis converts electrochemical gating into explicit statistical tests for independence, cooperativity, hidden substates, censoring, filtering sensitivity, and state recovery. The same formulation is applicable to OmpF, VDAC, OmpG, FhuA, OccK, and biomimetic nanopores in which functional closure may occur without complete steric occlusion.

Keywords: β-barrel channels; OmpF; electrochemical gating; hidden Markov model; single-channel recording; conductance heterogeneity; ion selectivity; nanopore transport.

Received: 23 August 2025
Accepted: 29 December 2025
Available online: 30 March 2026

1. Introduction

β-barrel membrane channels form aqueous pathways in Gram-negative bacterial outer membranes, mitochondria, chloroplasts, and several pore-forming toxin systems [1, 2, 3, 4]. Their large lumina enable passive transport of ions and small solutes, and their conductance can be resolved with high precision after reconstitution into planar lipid bilayers [5, 6, 7, 8]. A central unresolved question is how voltage drives these channels into low-conductance states when many of them lack the canonical voltage-sensor movements or well-defined occluded closed conformations familiar from several α-helical ion channels [9, 3, 10]. Single-channel records therefore contain information on both pore structure and electrochemical transport, but mean closure times capture only a small part of that information.

The outer membrane porin OmpF from *Escherichia coli* is a particularly useful system for resolving this problem because it is trimeric, electrically stable, and sensitive to pH, voltage polarity, lipid composition, electrolyte concentration, and ion identity [7, 8, 11, 12, 10]. Under sufficiently high applied voltage, a single trimer commonly exhibits current decreases in approximately one-third increments. The conductance levels are denoted here by L_0, L_1, L_2, and L_3, corresponding to zero, one, two, and three monomers in low-conductance configurations,

Cite as: Louis E. Brus (2026). State-Space Analysis of Hidden Low-Conductance States and Cooperative Electrochemical Gating in the Trimeric β-Barrel Channel OmpF. LC GC N. Am., 44(1) (2026) 01-07.

respectively [13, 14]. This pattern is compatible with independent closure of equivalent monomers, but the same trimeric arrangement also permits electrostatic, hydration-mediated, lipid-mediated, and allosteric coupling among monomers.

Recent OmpF measurements support an electrochemical view of gating rather than a purely steric view. In those recordings, first-monomer closure varied non-monotonically with electrolyte concentration; turnover concentrations depended on voltage polarity and cation identity; low-conductance states retained measurable current; and the fully low-conductance level exhibited inversion from cationic to anionic selectivity [14]. The concentration dependence can be described by screening-based scaling with high-concentration deviations, whereas the persistent residual conductance and selectivity inversion indicate that closure need not correspond to a single blocked-pore configuration [15, 14]. The remaining task is to determine whether the entire sequence $L_0 \to L_1 \to L_2 \to L_3$ follows independent monomer kinetics or a coupled state network with hidden low-conductance substates.

This distinction has direct mechanistic value. First, first-closure lifetimes do not determine the kinetics of the second and third closures. A first dwell-time distribution can appear simple even when later transitions are cooperative or multi-exponential [11, 14]. Second, the fully low-conductance level is not a zero-current state; its residual conductance can be large enough to support ion flow, and its selectivity can change sign relative to high-conductance states [15, 14]. These observations are difficult to explain by a single rigid occlusion, but they are consistent with electrochemical substates arising from local dewetting, surface-charge rearrangement, residue-network responses, or confined-electrolyte effects [16, 17, 18, 19, 20, 21].

The contribution of this article is a trajectory-level state-space analysis that links trimeric gating, current emissions, and selectivity changes in one statistical model. The analysis introduces an explicit independent-monomer reference with the testable $3:2:1$ transition-rate constraint, defines cooperativity factors for later closures, allows latent substates within L_3, and connects transition intensities to electrolyte concentration, voltage polarity, and cation identity. It also specifies validation criteria for filtering, event thresholds, censoring, insertion-level variability, and state recovery. These elements provide a quantitative route for deciding whether OmpF closure reflects independent monomer gating, cooperative closure, heterogeneous electrochemical substates, or a combination of these mechanisms.

2. Conceptual basis and problem formulation

2.1. From average dwell time to full state trajectories

Let $Y_r(t)$ denote the current recorded from replicate trajectory r under condition $x = (c, V, \gamma)$, where c is bulk electrolyte concentration, V is voltage polarity and magnitude, and γ denotes cation identity. Conventional first-closure analysis reduces each record to the time required for $L_0 \to L_1$. The state-space analysis instead represents the complete record by a latent state process

$$S_r(t) \in \mathscr{S} = \{L_0, L_1, L_2, L_3\}, \tag{1}$$

with optional expansion of the fully low-conductance level into substates $\{L_3^{(1)}, \ldots, L_3^{(H)}\}$. The observed current is modeled conditionally on the latent state:

$$Y_r(t) \mid S_r(t) = s \sim F_s\left\{\mu_s(x), \sigma_s^2(x), \theta_s\right\}, \tag{2}$$

where F_s may be Gaussian, Student-t, or a finite mixture distribution. The mean $\mu_s(x)$ represents the expected state current or conductance under the applied voltage, while $\sigma_s^2(x)$ captures open-channel noise, amplifier noise, finite filtering, and unresolved flicker. Robust emissions are preferred because brief current excursions and baseline fluctuations can otherwise be misclassified as additional biophysical states.

2.2. Continuous-time transition model

The state process is represented as a continuous-time Markov chain with generator $Q(x)$. For irreversible voltage-induced closure during a fixed voltage pulse, the dominant forward transition structure is

$$L_0 \xrightarrow{q_{01}(x)} L_1 \xrightarrow{q_{12}(x)} L_2 \xrightarrow{q_{23}(x)} L_3. \tag{3}$$

Brief reopening can be incorporated by adding reverse rates, but the forward-only form is sufficient for testing the primary closure sequence when reopening is rare or excluded by event criteria. If a trace ends before the next transition, the final residence time is right-censored rather than treated as a completed dwell. This distinction is important because voltage pulses often end before every channel has reached L_3, and ignoring censoring overestimates closure rates.

For state i, the likelihood contribution of a residence time t_i followed by transition $i \to j$ is

$$\ell_{ij} = \log q_{ij}(x) - \left\{\sum_{m \neq i} q_{im}(x)\right\} t_i, \tag{4}$$

whereas a right-censored residence time contributes only the survival term

$$\ell_i^{\text{cens}} = -\left\{\sum_{m \neq i} q_{im}(x)\right\} t_i. \tag{5}$$

These likelihood terms allow later-state kinetics to be estimated from the same current traces that provide first-closure dwell times.

2.3. Independent-monomer null model

If each open monomer has the same condition-dependent closure rate $\lambda(x)$, and if the three monomers close independently, the transition rate from a state with k low-conductance monomers to a state with $k+1$ low-conductance monomers equals the number of remaining high-conductance monomers multiplied by $\lambda(x)$:

$$q_{k,k+1}(x) = (3-k)\lambda(x), \qquad k = 0, 1, 2. \tag{6}$$

The observable prediction is therefore

$$q_{01} : q_{12} : q_{23} = 3 : 2 : 1. \tag{7}$$

This ratio is independent of the absolute closure rate, the electrolyte-scaling equation, and cation identity. It requires only exchangeable monomers and kinetic independence. Because current records do not identify which physical monomer has closed, eq. (7) is valuable: it tests independence from residence times of observable conductance levels without requiring monomer-specific labeling.

2.4. Cooperativity factors

Cooperative closure is represented by

$$q_{k,k+1}(x) = (3-k)\lambda(x)\eta_k(x), \qquad \eta_0(x) = 1, \tag{8}$$

where η_1 and η_2 quantify how one or two prior closures affect subsequent closure. Values $\eta_k > 1$ indicate positive cooperativity, values $\eta_k < 1$ indicate negative cooperativity or stabilization of the remaining high-conductance monomers, and $\eta_k = 1$ recovers the independent-monomer case. Condition dependence can be written as

$$\log \eta_k(x) = \alpha_{k0} + \alpha_{kV}\mathbb{I}(V<0) + \alpha_{k\gamma} + f_k(\log c) + \alpha_{kV\gamma}\mathbb{I}(V<0)\mathbb{I}(\gamma), \tag{9}$$

where f_k can be a spline or a constrained electrolyte function. This parameterization tests whether polarity, concentration, and cation identity alter the full state network rather than merely rescaling the first closure.

2.5. Coupling to electrochemical concentration scaling

The first-closure rate can be coupled to electrolyte concentration through

$$\lambda(c,V,\gamma) = \lambda_{0,V,\gamma}\left[-\frac{X}{2c_{\mathrm{eff}}(c,\gamma)} + \sqrt{\frac{X^2}{4c_{\mathrm{eff}}(c,\gamma)^2}+1}\right]^{-n_{V,\gamma}}, \tag{10}$$

with

$$c_{\mathrm{eff}}(c,\gamma) = \frac{c}{1+\left(c/K_{D,\gamma}\right)^2}. \tag{11}$$

Here X is an effective fixed-charge concentration, n is an apparent gating charge, and K_D controls the onset of high-concentration deviation from ideal screening. In the full state model, λ governs the baseline tendency toward first closure, whereas η_1, η_2, and the emission distributions determine whether later states follow the same electrochemical dependence or enter distinct low-conductance substates.

2.6. Hidden heterogeneity in the fully low-conducting state

The broad variation of L_3 conductance and selectivity motivates a mixture emission:

$$p(Y \mid L_3, x) = \sum_{h=1}^{H} \pi_h(x) F_{3h}\left\{\mu_{3h}(x), \sigma_{3h}^2(x)\right\}, \tag{12}$$

where $H = 1$ represents one low-conductance state with measurement noise, and $H > 1$ represents several latent substates. When reversal-potential measurements are available, current and selectivity can be modeled jointly:

$$p\{Y, \rho_{\mathrm{sel}} \mid L_3, x\} = \sum_{h=1}^{H} \pi_h(x) F_{3h}(Y) G_{3h}(\rho_{\mathrm{sel}}), \tag{13}$$

where

$$\rho_{\mathrm{sel}} = \log\left(\frac{P_{\mathrm{Cl}}}{P_{\mathrm{cat}}}\right). \tag{14}$$

A positive ρ_{sel} denotes anion preference, and a negative ρ_{sel} denotes cation preference. The joint model is essential because similar residual currents can arise from substates with different ion preference. Selectivity inversion is therefore assigned to latent states rather than averaged across all fully low-conductance events.

3. Materials and methods

3.1. Empirical setting

The analysis is specified for single OmpF trimer recordings after reconstitution into planar lipid bilayers by a Montal–Mueller-type protocol [22, 14]. The relevant experimental design uses symmetric chloride salts buffered near pH 6, voltage-clamp recordings at ±200 mV for gating kinetics, KCl concentrations spanning low millimolar to molar conditions, and cation comparisons using NaCl, LiCl, and CsCl [14]. Current records used to estimate first-closure dwell times contain the information needed to recover residence times and transitions among L_0, L_1, L_2, and L_3. Conductance and concentration-gradient measurements provide complementary emission variables for testing whether low-conductance states differ only in amplitude or also in ion preference [23, 15, 14].

3.2. Signal preprocessing and event detection

Raw traces should be corrected for slow drift using baseline segments recorded immediately before channel insertion or before voltage steps. The filtering frequency used for inference must be reported because excessive filtering can merge short closures, whereas insufficient filtering can inflate state counts through high-frequency noise. The primary analysis follows the event-threshold convention used in OmpF gating measurements by excluding events shorter than 20 ms, which separates slower voltage-induced gating from fast flicker [14]. Sensitivity analyses should repeat the inference at 10 ms and 50 ms. State amplitudes can be initialized from current-level histograms and refined by hidden Markov or constrained change-point estimation.

3.3. State segmentation

Two segmentation strategies are appropriate. The first is a constrained change-point procedure in which current levels are assigned to monotonic closure states according to approximate one-third current decrements. This approach is transparent and easy to audit. The second is hidden Markov segmentation, in which the state sequence is inferred jointly with emission means and variances [24, 25, 26]. Hidden Markov segmentation is preferable when state boundaries are noisy, brief reopening occurs, or L_3 contains latent substates. State labels should be evaluated using posterior state probabilities, recovery simulations under fitted noise and filtering, and visual overlay on representative current records. Figure 1 shows how a trace-level current record is converted into assigned states for kinetic estimation.

3.4. Model hierarchy

The model hierarchy is summarized in table 1. Each increase in complexity corresponds to a specific biophysical claim. The independent continuous-time model tests exchangeability and independence. The cooperative model tests whether earlier closure accelerates or slows later closure. The hidden-substate model tests whether L_3 is heterogeneous beyond measurement noise. The semi-Markov model tests whether residence-time distributions depart from memoryless kinetics.

Table 1: Model hierarchy for trajectory-level OmpF gating analysis.

Model	Constraint	Biophysical question
Independent CTMC	$q_{01} : q_{12} : q_{23} = 3 : 2 : 1$	Do the three monomers close independently under a shared closure rate?
Cooperative CTMC	$q_{k,k+1} = (3-k)\lambda\eta_k$	Does closure of one monomer alter the rate of subsequent closures?
Condition-dependent CTMC	λ, η_1, and η_2 depend on c, V, and cation	Does electrolyte composition reshape the full state network rather than only first closure?
Hidden-substate HMM	$L_3 = \{L_3^{(1)}, \ldots, L_3^{(H)}\}$	Is the fully low-conductance level a single noisy state or a family of substates?
Semi-Markov model	Non-exponential residence-time distributions	Are residence times inconsistent with a memoryless transition process?
Joint conductance–selectivity model	Current and permeability ratio are modeled together	Which low-conductance states account for selectivity inversion?

3.5. Model selection and uncertainty

Models should be compared using likelihood-based criteria, insertion-level bootstrap, and held-out predictive performance. Akaike and Bayesian information criteria are useful for initial comparison, but a mixture model should be retained only if it produces stable state assignments, biologically interpretable emission means, non-degenerate mixture weights, and reproducible parameters across independent channel insertions. Confidence intervals for η_1, η_2, K_D, n, and mixture weights should be obtained by resampling complete insertions rather than individual events, because events from the same channel are statistically dependent. Validation is strengthened by testing whether fitted models recover the L_0, L_1, L_2, and L_3 step pattern, reproduce the reported concentration dependence of first closure, predict held-out dwell-time distributions, and recover generated state sequences sampled and filtered like the experimental traces.

3.6. Robustness checks

Trajectory-level ion-channel inference is sensitive to thresholding, filtering, censoring, and pooling decisions. Table 2 lists the minimum checks needed before interpreting cooperativity or hidden substates as biophysical effects.

4. Analytical results and testable predictions

4.1. The trimeric null model is identifiable from state residence times

Independence can be tested without knowing which physical monomer has closed. Because the three monomers are indistinguishable in the current trace, conductance steps alone cannot assign a transition to monomer A, B, or C. Nevertheless, the independent model predicts a unique sequence of state-level rates. If the mean residence times in L_0, L_1, and L_2 are $\bar{t}_0$, $\bar{t}_1$, and $\bar{t}_2$, then under the independent irreversible model

$$\mathbb{E}[\bar{t}_0] = \frac{1}{3\lambda}, \qquad \mathbb{E}[\bar{t}_1] = \frac{1}{2\lambda}, \qquad \mathbb{E}[\bar{t}_2] = \frac{1}{\lambda}. \tag{15}$$

Equivalently,

$$\bar{t}_0 : \bar{t}_1 : \bar{t}_2 = \frac{1}{3} : \frac{1}{2} : 1. \tag{16}$$

A pattern in which $\bar{t}_1$ or $\bar{t}_2$ is shorter than predicted indicates positive cooperativity, whereas longer residence times indicate that earlier closure stabilizes the remaining high-conductance monomers. This test is stronger than comparison of first-closure times alone because it uses the complete trimeric trajectory. The current trace and state strip in fig. 1 show the residence intervals required for this calculation.

4.2. Electrolyte concentration can affect first closure and cooperativity separately

The biphasic concentration dependence of first-monomer closure can be represented by eqs. (10) and (11). However, the same first-closure time can arise from different state networks. One condition may show rapid first closure followed by slow completion to L_3, whereas another may show slower first closure but strong acceleration of later closure. These cases are indistinguishable if the analysis stops at τ_0, but they imply different electrochemical mechanisms. The state-network model therefore separates the first-closure tendency $\lambda(c,V,\gamma)$ from conditional coupling $\eta_1(c,V,\gamma)$ and $\eta_2(c,V,\gamma)$. This separation is especially important near turnover concentrations, where screening, ion pairing, finite ion size, hydration, and nanoconfinement can compete [27, 28, 29].

4.3. Multiple L_3 substates explain conductance and selectivity dispersion

If L_3 is a single physical state, its conductance and selectivity measurements should be described by one emission distribution after accounting for measurement noise and insertion-level variability. A broad unimodal distribution would support one noisy low-conductance state. Reproducible multimodality in conductance, selectivity, or their joint distribution would instead support a family of electrochemically distinct substates. Such a result is consistent with electrochemical gating because different local dewetting sites, residue-network configurations, or hydration barriers could reduce current without producing the same ion preference. The mixture model in eq. (13) therefore provides an operational test of whether OmpF closure produces one low-conductance state or several low-conductance states.

4.4. Selectivity inversion should be assigned to latent states

The reversal from cationic selectivity in L_0, L_1, and L_2 to anionic selectivity in L_3 is one of the most informative observations in OmpF gating [15, 14]. Joint state-space analysis can determine whether the inversion is present across all L_3 events or concentrated in a subset of $L_3^{(h)}$ substates. Concentration of the inversion in a subset would show that fully low-conductance events are not equivalent and that selectivity inversion is controlled by specific electrochemical configurations rather than by simple loss of cross-sectional area. This distinction separates steric occlusion from dewetting, hydration-barrier, and residue-network mechanisms.

4.5. Condition-dependent state networks avoid misleading single-axis rankings

Cation identity and concentration can interact non-monotonically. Classifying salts by a single ranking at one concentration can therefore be misleading. A state-space representation avoids this problem by estimating separate condition-dependent quantities: λ for first closure, η_k for cooperativity, π_h for hidden-substate prevalence, and emission parameters for conductance and selectivity. A salt that accelerates first closure may not accelerate completion to L_3, and a salt that increases L_3 occupancy may not produce the same selectivity inversion. This multidimensional interpretation is more compatible with nanoconfined electrolyte physics than a one-dimensional Hofmeister ordering [30, 28, 14]. Figures 2 and 3 summarize the kinetic and validation signatures expected under these alternatives.

5. Discussion

5.1. Mechanistic value of state-space analysis

The electrochemical-gating view holds that OmpF closure does not require a single large steric occlusion. Voltage can perturb charge distributions, hydration structure, and hydrophobic regions inside the pore, producing local barriers that reduce ionic flux while preserving measurable conductance [14]. State-space analysis strengthens this interpretation by defining the quantitative signatures expected for cooperative and heterogeneous gating. A first-closure lifetime cannot determine whether the trimer closes independently; the complete sequence of residence times can. A single residual-conductance average cannot determine whether L_3 is homogeneous; a joint conductance–selectivity emission model can. A single cation ranking cannot establish a universal ion effect; condition-dependent transition intensities can.

The central prediction is the $3:2:1$ transition-rate ratio. Agreement with this ratio would support independent exchangeable monomers under the tested condition. Faster later closures would indicate pos-

Table 2: Validation checks for state-space analysis of OmpF gating.

Concern	Analysis	Interpretation standard
Fast flicker versus gating	Repeat inference after excluding events shorter than 10, 20, and 50 ms	Cooperativity and substate conclusions should not depend on a single threshold.
Filtering artifacts	Repeat segmentation after alternative low-pass filters compatible with time resolution	State counts should remain stable within uncertainty.
Pooling across insertions	Fit hierarchical or leave-one-insertion-out models	Effects should not be driven by a single channel insertion.
Overfitting of L_3 mixtures	Compare $H = 1,2,3$ using bootstrap and predictive checks	Additional substates must improve prediction and have reproducible means.
Censored dwell times	Include right-censoring when voltage is removed before a transition	Transition rates should not be biased by protocol termination.
State recovery	Generate traces with fitted noise, filtering, and sampling rate	The analysis should recover known states and transition rates within uncertainty.
Voltage-polarity asymmetry	Fit separate and shared-parameter polarity models	Polarity effects should be reported with confidence intervals.
Cation-dependent effects	Estimate cation-specific K_D, λ, and η_k	Ion effects should not be reduced to a single Hofmeister ranking without concentration context.

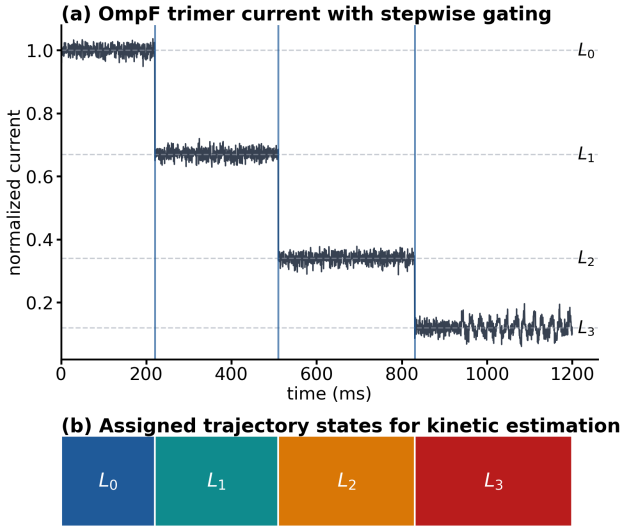

Figure 1: Trajectory-level current analysis for voltage-induced OmpF gating. Panel (a) shows a single-trimer current record with successive occupancy of L_0, L_1, L_2, and L_3; the low-current portion illustrates residual fluctuations compatible with unresolved low-conductance substates. Panel (b) shows the assigned latent-state intervals used to estimate residence times, transition intensities, cooperativity factors, and state-specific current emissions.

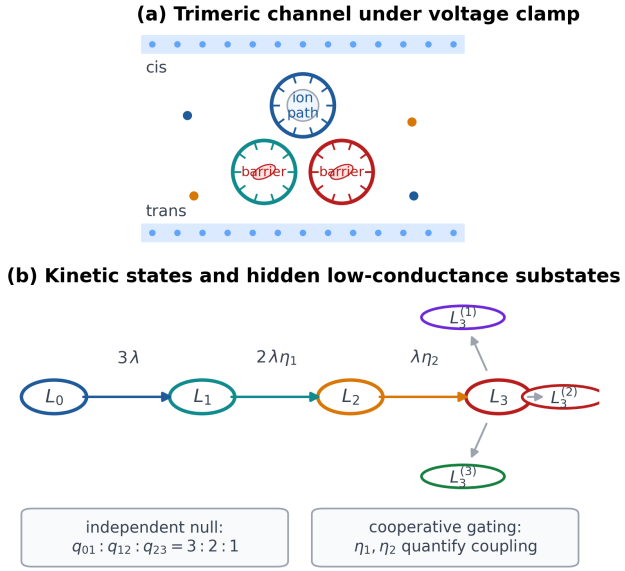

Figure 2: Trimeric state model for OmpF closure. Panel (a) depicts a single trimer in a planar bilayer with one high-conductance monomer and two low-conductance monomers. Panel (b) gives the corresponding state network. The independent-monomer model requires $q_{01} : q_{12} : q_{23} = 3 : 2 : 1$, whereas the cooperative model estimates η_1 and η_2 for later closures. The fully low-conductance state can be partitioned into latent substates with different conductance and selectivity emissions.

itive coupling, possibly through electrostatic rearrangement, local dehydration, or lipid-mediated changes induced by the first closure. Slower later closures would indicate negative coupling or stabilization of remaining high-conductance monomers. Because η_1 and η_2 are condition-dependent, the same channel can exhibit different coupling regimes across salt type, concentration, and voltage polarity.

5.2. Relation to hydrophobic gating and nanoconfined electrolyte physics

Hydrophobic gating explains voltage- or geometry-dependent wetting transitions in biological and biomimetic nanopores [19, 17, 18, 20, 21]. In such systems, a pore can become functionally low-conducting without a rigid physical plug because water and ions encounter a local free-energy barrier. Concentrated electrolytes add further complexity because screening can become non-classical under confinement, and ion correlations, hydration, ion pairing, and finite-size effects can modify transport in ways not captured by dilute-solution intuition [27, 31, 28, 29]. A hidden-state formulation matches this physical picture. It permits several low-conductance substates rather than forcing all closures into one structural state, and it allows the prevalence of those substates to change with cation identity and concentration.

5.3. Implications for earlier interpretations of OmpF and related pores

Mutation, loop-tethering, and environmental-modulation studies show that voltage gating in OmpF is robust: many perturbations alter closure kinetics or critical voltage, but none provides a universal switch that

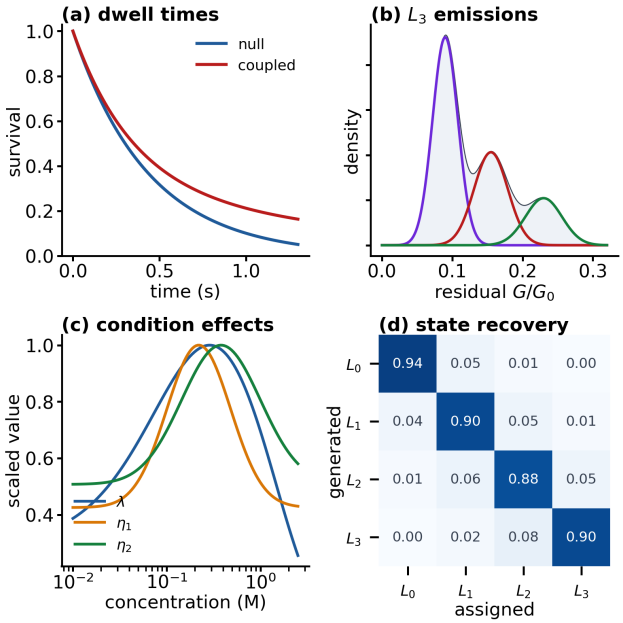

Figure 3: Model-based diagnostic outputs for trajectory-level OmpF gating analysis. Panel (a) compares the residence-time survival expected under an independent continuous-time model with a heavier-tailed coupled process. Panel (b) shows how multimodal L_3 emissions separate low-conductance substates. Panel (c) illustrates that first closure λ and cooperativity factors η_1, η_2 can have different concentration dependences. Panel (d) displays a state-recovery check used to determine whether segmentation accurately recovers the known state sequence under the fitted sampling, noise, and filtering conditions.

eliminates the phenomenon under all conditions [13, 11, 10, 14]. Robust gating is expected if several electrochemical pathways can produce low current. The same reasoning applies to other β-barrel systems, including VDAC, OmpG, FhuA, and OccK, where low-conductance states, loop motions, electrostatic effects, and selectivity changes vary by system [9, 32, 33, 34, 35]. The state-space model does not require identical structural mechanisms across pores. It supplies common statistical tests for independence, cooperativity, homogeneity, and hidden heterogeneity.

5.4. Practical advantages for single-channel analysis

The analysis has several practical advantages. First, it reduces overreliance on pooled dwell-time histograms by preserving insertion-level variation. Second, it separates amplitude classification from kinetic inference, reducing bias when conductance levels overlap. Third, it treats voltage termination as censoring rather than as a spontaneous transition. Fourth, it provides checks against false detection of substates caused by filtering or noise. Finally, it integrates current amplitude with reversal-potential-derived selectivity, which is essential when low-conductance states remain permeable and change ion preference.

5.5. Limitations

The analysis requires raw or event-level current traces. Published aggregate values, such as mean first-closure lifetimes and average conductances, are sufficient to motivate the model but not to estimate all transition intensities, cooperativity factors, or hidden-substate weights. The model also relies on identifiable conductance levels; severe overlap between states or extensive unresolved flicker can reduce precision. These limitations can be addressed by reporting posterior state probabilities, performing threshold and filter sensitivity analyses, using recovery simulations, and fitting hierarchical models that account for insertion-level variation. The method should therefore be interpreted as a rigorous trajectory-level analysis of well-controlled recordings, not as a substitute for experimental replication.

6. Conclusions

A mechanistic account of OmpF voltage-induced closure requires the complete sequence of conductance states, not only the average time to first monomer closure. The trimeric structure provides a direct reference condition: independent monomers must produce transition rates in the ratio $3:2:1$. Departures from this ratio quantify cooperativity and reveal whether prior closure accelerates or stabilizes the remaining monomers. The finite residual conductance and selectivity inversion of the fully low-conductance state justify a hidden-substate emission model that determines whether L_3 is one noisy state or a family of electrochemical substates. Coupling these components to concentration, voltage polarity, and cation identity yields falsifiable trajectory-level tests for electrochemical gating. The analysis is feasible with standard single-channel OmpF recordings and extends naturally to other β-barrel channels and biomimetic nanopores in which functional closure may occur without a unique steric closed structure.

References

[1] Hille, B. (2001). *Ion channels of excitable membranes* (3rd ed.). Sinauer Associates.
[2] Nikaido, H. (2003). Molecular basis of bacterial outer membrane permeability revisited. *Microbiology and Molecular Biology Reviews*, *67*, 593–656.
[3] Delcour, A. H. (2015). *Electrophysiology of unconventional channels and pores*. Springer International Publishing.
[4] Chaturvedi, D., & Mahalakshmi, R. (2017). Transmembrane β-barrels: Evolution, folding and energetics. *Biochimica et Biophysica Acta - Biomembranes*, *1859*, 2467–2482.
[5] Benz, R., Janko, K., Boos, W., & Lauger, P. (1978). Formation of large, ion-permeable membrane channels by the matrix protein (porin) of *Escherichia coli*. *Biochimica et Biophysica Acta*, *511*, 305–319.
[6] Delcour, A. H. (2002). Structure and function of pore-forming beta-barrels from bacteria. *Journal of Molecular Microbiology and Biotechnology*, *4*, 1–10.
[7] Alcaraz, A., Nestorovich, E. M., Aguilella-Arzo, M., Aguilella, V. M., & Bezrukov, S. M. (2004). Salting out the ionic selectivity of a wide channel: The asymmetry of OmpF. *Biophysical Journal*, *87*, 943–957.
[8] Nestorovich, E. M., Rostovtseva, T. K., & Bezrukov, S. M. (2003). Residue ionization and ion transport through OmpF channels. *Biophysical Journal*, *85*, 3718–3729.
[9] Colombini, M. (1989). Voltage gating in the mitochondrial channel, VDAC. *Journal of Membrane Biology*, *111*, 103–111.
[10] Nestorovich, E. M., & Bezrukov, S. M. (2023). Beta-barrel channel response to high electric fields: Functional gating or reversible denaturation? *International Journal of Molecular Sciences*, *24*, 16655.
[11] Perini, D. A., Alcaraz, A., & Queralt-Martin, M. (2019). Lipid headgroup charge and acyl chain composition modulate closure of bacterial β-barrel channels. *International Journal of Molecular Sciences*, *20*, 674.
[12] Liko, I., Degiacomi, M. T., Lee, S., Newport, T. D., Gault, J., Reading, E., Hopper, J. T. S., Housden, N. G., White, P., Colledge, M., Sula, A., Wallace, B. A., Kleanthous, C., Stansfeld, P. J., Bayley, H., Benesch, J. L. P., Allison, T. M., & Robinson, C. V. (2018). Lipid binding attenuates channel closure of the outer membrane protein OmpF. *Proceedings of the National Academy of Sciences of the United States of America*, *115*, 6691–6696.
[13] Basle, A., Iyer, R., & Delcour, A. H. (2004). Subconductance states in OmpF gating. *Biochimica et Biophysica Acta*, *1664*, 100–107.
[14] Alvero-Gonzalez, L. M., Perini, D. A., Lopez, M. L., Alcaraz, A., & Queralt-Martin, M. (2026). Voltage-induced closure of β-barrel channels as electrochemical gating. *Bioelectrochemistry*, *169*, 109181.
[15] Alcaraz, A., Nestorovich, E. M., Lopez, M. L., Garcia-Gimenez, E., Bezrukov, S. M., & Aguilella, V. M. (2009). Diffusion, exclusion, and specific binding in a large channel: A study of OmpF selectivity inversion. *Biophysical Journal*, *96*, 56–66.
[16] Baek, S., Kwon, S. R., & Bohn, P. W. (2022). Potential-induced wetting and dewetting in hydrophobic nanochannels for mass transport control. *Current Opinion in Electrochemistry*, *34*, 100980.
[17] Trick, J. L., Song, C., Wallace, E. J., & Sansom, M. S. P. (2017). Voltage gating of a biomimetic nanopore: Electrowetting of a hydrophobic barrier. *ACS Nano*, *11*, 1840–1847.
[18] Trick, J. L., Aryal, P., Tucker, S. J., & Sansom, M. S. P. (2015). Molecular simulation studies of hydrophobic gating in nanopores and ion channels. *Biochemical Society Transactions*, *43*, 146–150.

[19] Beckstein, O., Biggin, P. C., & Sansom, M. S. P. (2001). A hydrophobic gating mechanism for nanopores. *Journal of Physical Chemistry B*, *105*, 12902–12905.
[20] Aryal, P., Sansom, M. S. P., & Tucker, S. J. (2015). Hydrophobic gating in ion channels. *Journal of Molecular Biology*, *427*, 121–130.
[21] Seiferth, D., Biggin, P. C., & Tucker, S. J. (2022). When is a hydrophobic gate not a hydrophobic gate? *Journal of General Physiology*, *154*, e202213210.
[22] Montal, M., & Mueller, P. (1972). Formation of bimolecular membranes from lipid monolayers and a study of their electrical properties. *Proceedings of the National Academy of Sciences of the United States of America*, *69*, 3561–3566.
[23] Hodgkin, A. L., & Katz, B. (1949). The effect of sodium ions on the electrical activity of the giant axon of the squid. *Journal of Physiology*, *108*, 37–77.
[24] Becker, J. D., Honerkamp, J., Hirsch, J., Frobe, U., Schlatter, E., & Greger, R. (1994). Analysing ion channels with hidden Markov models. *Pflugers Archiv*, *426*, 328–332.
[25] Venkataramanan, L., & Sigworth, F. J. (2002). Applying hidden Markov models to the analysis of single ion channel activity. *Biophysical Journal*, *82*, 1930–1942.
[26] Qin, F. (2004). Restoration of single-channel currents using the segmental k-means method based on hidden Markov modeling. *Biophysical Journal*, *86*, 1488–1501.
[27] Smith, A. M., Lee, A. A., & Perkin, S. (2016). The electrostatic screening length in concentrated electrolytes increases with concentration. *Journal of Physical Chemistry Letters*, *7*, 2157–2163.
[28] Elliott, G. R., Gregory, K. P., Robertson, H., Craig, V. S. J., Webber, G. B., Wanless, E. J., & Page, A. J. (2024). The known-unknowns of anomalous underscreening in concentrated electrolytes. *Chemical Physics Letters*, *843*, 141190.
[29] Aluru, N. R., Aydin, F., Bazant, M. Z., Blankschtein, D., Brozena, A. H., de Souza, J. P., Elimelech, M., Faucher, S., Fourkas, J. T., Koman, V. B., Kuehne, M., Kulik, H. J., Li, H.-K., Li, Y., Li, Z., Majumdar, A., Martis, J., Misra, R. P., Noy, A., Pham, T. A., Qu, H., Rayabharam, A., Reed, M. A., Ritt, C. L., Schwegler, E., Siwy, Z., Strano, M. S., Wang, Y., Yao, Y.-C., Zhan, C., & Zhang, Z. (2023). Fluids and electrolytes under confinement in single-digit nanopores. *Chemical Reviews*, *123*, 2737–2831.
[30] Gregory, K. P., Elliott, G. R., Robertson, H., Kumar, A., Wanless, E. J., Webber, G. B., Craig, V. S. J., Andersson, G. G., & Page, A. J. (2022). Understanding specific ion effects and the Hofmeister series. *Physical Chemistry Chemical Physics*, *24*, 12682–12718.
[31] Lee, A. A., Perez-Martinez, C. S., Smith, A. M., & Perkin, S. (2017). Underscreening in concentrated electrolytes. *Faraday Discussions*, *199*, 239–259.
[32] Choudhary, O. P., Ujwal, R., Kowallis, W., Coalson, R., Abramson, J., & Grabe, M. (2010). The electrostatics of VDAC: Implications for selectivity and gating. *Journal of Molecular Biology*, *396*, 580–592.
[33] Liu, J., Eren, E., Vijayaraghavan, J., Cheneke, B. R., Indic, M., van den Berg, B., & Movileanu, L. (2012). OccK channels from *Pseudomonas aeruginosa* exhibit diverse single-channel electrical signatures but conserved anion selectivity. *Biochemistry*, *51*, 2319–2330.
[34] Thakur, A. K., & Movileanu, L. (2019). Real-time measurement of protein-protein interactions at single-molecule resolution using a biological nanopore. *Nature Biotechnology*, *37*, 96–101.
[35] Zhuang, T., & Tamm, L. K. (2014). Control of the conductance of engineered protein nanopores through concerted loop motions. *Angewandte Chemie International Edition*, *53*, 5897–5902.